# Fabrication of energy-efficient carbonate-based cementitious material using sodium meta-aluminate activated limestone powder

Fan Wang[1], Guangcheng Long[*1], Jionghuang He[1], Youjun Xie[1], Zhuo Tang[1], Xiang Zhou[1], Min Bai[1], John L. Zhou[12]

[1] School of Civil Engineering, Central South University, 68 South Shaoshan Road, Changsha, Hunan 410075, China

[2] Centre for Green Technology, School of Civil and Environmental Engineering, University of Technology Sydney, Sydney, NSW 2007, Australia

Fan Wang, Email: wn2020@csu.edu.cn

Guangcheng Long, Email: longguangcheng@csu.edu.cn

Jionghuang He, Email: hjh2017@foxmail.com

Youjun Xie, Email: xieyj@csu.edu.cn

Zhuo Tang, Email: Zhuo.Tang-1@alumni.uts.edu.au

Xiang Zhou, Email: xiangzhou@csu.edu.cn

Min Bai, Email: 1983857921@qq.com

John L. Zhou, Email: junliang.zhou@uts.edu.au

[*] Corresponding author: longguangcheng@csu.edu.cn (G. Long)

## ABSTRACT

Limestone powder (LP) and sodium meta-aluminate (SMA) were used to fabricate calcium carbonate-based cementitious material, as a solution to address the solid waste problem. The effects of SMA doses and curing conditions on the hydration properties and mechanical performance of paste were investigated. The results show that the 28-d unconfined compressive strength and flexural strength of paste with a LP/SMA ratio of 2/1 were 49.7 MPa and 15.9 MPa, respectively. The characterization by SEM, XRD and TG shows that the calcium aluminum carbonate hydroxide hydrate (CACHH) was the predominant hydrated product and had a dense layered double hydroxides structure ($LDH_S$). The micro-bridge effect developed by LDHs significantly increases the flexural strength of the paste. Meanwhile, the developed paste exhibited an extremely low carbon emission and energy consumption. This study also reveals the mechanism of LP incorporating with SMA to form CACHH. Overall, this work provides an approach of high value-added utilization for LP as a binder without tedious operation, which could address carbon emission reduction and circular economy of LP.



*Keywords:* Solid waste; Limestone powder; Calcium carbonate-based cementitious material; High value utilization; Microstructure

## INTRODUCTION

Calcium carbonate ($CaCO_3$) as an indispensable calcareous mineral widely exists in nature with abundant reserves. $CaCO_3$ not only constitutes an important part of rock minerals, but also is the main component of animal bones or shells, [1-3] therefore playing a key role in the global carbon cycle.[4] In addition, calcium carbonate is often used as an architecture for investigating the crystallization and nucleation of ionic-solutions.[5-7] In the field of construction, calcium carbonate has been widely used in plastic, building materials, adhesives and sealing materials.[8-11] In term of the production and use of calcium carbonate, China's annual output had exceeded 30 million tons in the last five years. In 2019, its output reached 35.95 million tons, accounting for 28.8% of the global output.[12]

Nevertheless, it is inevitable that the exploitation of calcium carbonate produces a large amount of solid waste. As a result, the safe disposal of these massive solid waste has become an issue of great concern.[4,9] Meanwhile, the cement industry has been facing tremendous pressure to reduce energy consumption and greenhouse gas emissions, which prompts the search for alternative and sustainable materials for achieving such objectives.[13-15] The utilization of limestone powder (LP) has attracted extensive attention because of its low price and low environmental stress.[16] The incorporation of LP has a positive synergistic effect on the early strength, hydration process, durability and microstructure of concrete.[17-21] Therefore, it is a win-win solution to use LP to replace cement for preparing cementitious materials.

LP can affect the properties of cementitious composites via physical effects (e.g., micro-aggregate filling, dilution and nucleation of microcrystals) and chemical effects.[22-25] In cement, LP with certain fineness could accelerate microcrystalline nucleation effect to improve the mechanical properties of concrete.[26-29] On the other hand, the hydration of $C_3A$ promotes the dissolution of LP, which regulate the reaction between Ca/Si in C-S-H gel and $C_3S$ to produce hydrated calcium carbo-silicate.[30-31] As

a result, the use of LP as a partial replacement for cement has been reported to improve not only the workability of concrete, but also its strength and impermeability.[14] It should be noted that the limit of substitution is always set at around 10-50% to avoid the excessive LP reducing the workability of cementitious material (although larger amounts are sometimes used).[32]

Therefore, scholars attempted to further expand this limit by creating adhesives made almost entirely from waste to achieve 100% substitution. [33] In recent years, preliminary results have been achieved in the preparation of alkali-activated cement in which LP was used as the only precursor. [34] When LP is dissolved in an alkaline media, the formation of new phases may be caused by the recrystallization of LP. Simultaneously, the carbonization of $Ca^{2+}$ by $CO_2$ induces a dense structure of the matrix, which facilitates the strength development. Scholars have used marble sludge 100% replacement cement and combined with Na and Si to successfully prepared (N)-C-S-H gels in alkaline sodium silicate solution.[35] These methods reduce carbon emissions, eliminates the need for conventional heat treatment and has a significant economic benefit. However, the strength of formed cementitious materials increases slowly, which is not conducive to engineering practice.

The development of carbon-aluminate system also provided a new perspective for the utilization of LP.[36-38] Previous studies have employed calcium carbonate with aluminum phases to produce mono-carbo-aluminate (mono-carbon ettringite).[39-42] This product belongs to the family of layered double hydroxides (LDHs) and exhibits the superior thermal stability.[43] Therefore, the calcium carbonate-based cementitious materials can realize both 100% replacement of cement and high-value utilization of LP in some specific conditions. However, increasing the utilization of LP significantly sacrifices the mechanical properties of the substrate. Therefore, how to achieve the synergistic development of high value-added utilization, low-energy consumption and high structure performance is the main issue facing the resourceful processing of LP.

The aim of this study is to use fine LP (800 meshes) to fabricate calcium carbonate-based cementitious material based on a simple chemical method, in which tedious operation such as high-temperature calcination or mechanical modification is avoided. The effects of various LP/SMA ratios and different curing conditions on the micro-structure and macro-mechanical properties of paste were analyzed. X-ray diffraction (XRD), scanning electron microscopy (SEM), thermal gravimetry and derivative thermal gravimetry (TG-DTG) techniques were used to examine the composition and morphology of hydrated products. This research results provide a new simple approach for the high-value utilization of limestone powder and an important reference for the research of calcium carbonate-based cementitious material.

## MATERIALS AND METHODS

### Experimental materials

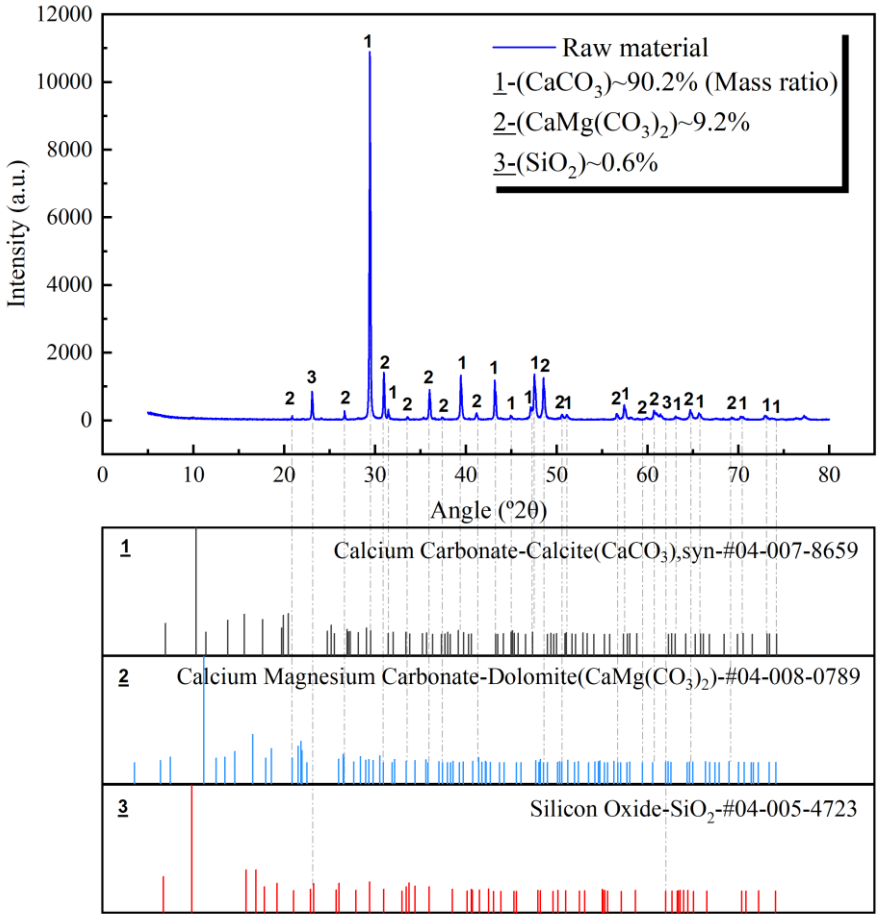


**Fig. 1.** The XRD results of LP. (1) calcium carbonate, (2) calcium magnesium carbonate and (3) silicon oxide.

In this study, calcium carbonate-based cementitious material was prepared using LP with particle fineness of 800 meshes (<15 μm) and a density of 2500 kg/m$^3$. The LP was sourced from a calcium carbonate manufacturer in Jiangxi, China. The loss on ignition of LP reached 41.51% at 950℃. The minerals composition of LP was detected by XRD (as shown in Fig. 1. The result demonstrates that LP mainly consists of calcite, dolomite, and silicon oxide, whose mass ratios are 90.2%, 9.2%, and 0.6% respectively. Other materials were included deionized water and industrial grade sodium meta-aluminate (SMA) with a purity of 98% (Sinopharm Group).

**Experimental design**

The specific design scheme is presented in Table 1. The calcium carbonate-based cementitious material was prepared with different LP/SMA mass ratios (i.e., 10:1, 7.5:1 ,5:1, 3:1, 2:1 and 1:1). Meanwhile, the curing condition as another major factor was considered. Specifically, three curing conditions were designed, which included indoor curing (IC) at 20±2°C and relative humidity of 60±3%, standard curing (SC) at a temperature of 20±2°C and relative humidity of 95±3%, and steam curing (SC-60 °C) at a constant temperature of 60±2℃ through the steam curing equipment. The deionized water was used as an aqueous solution for participating in the hydration, and the water solid ratio was set at 0.3 for all mixtures.

**Table 1. Specific design scheme of different ratios of LP to SMA**

| Factors | Details |
|---|---|
| Ratio of LP/SMA | A (10:1); B (7.5:1); C (5.0:1); D (3.0:1); E (2.0:1); F (1.0:1) |
| Curing conditions | IC (Indoor curing); SC (Standard curing); SC-60 ℃ (Steam curing) |
| Solutions | Deionized water |
| Water solid ratio | 0.3 |

**Sample preparation**

At first, LP was uniformly mixed with SMA in different proportions and stirred vigorously with agitator at 300 rad/min for 3 minutes. Then the deionized water was slowly added to the mixture under the agitation of 600 rad/min for 5 minutes. The prepared paste was then molded into 40 mm

(length)×40 mm (width)×40 mm (thickness) and 160 mm (length)×40 mm (width)×40 mm (thickness) plastic molds coated with a thin layer of lubricating oil for the subsequent demolding. Finally, a plastic film was used to encapsulate the mold to prevent the external interference and moisture evaporation. When the samples were demolded after 1 day of molding, and then cured to the tested age under the designed curing conditions.

## Characterization

### Unconfined compressive strength (UCS) and flexural strength (FS)

At scheduled test ages (i.e., 3, 14 and 28 days), the specimens were taken out and kept dry before strength (UCS, FS) measurements. The FS was measured via a servo press with a vertical loading rate of 50 N/s. The broken specimens were then collected along with other prepared cubic samples for further testing of the UCS with a loading rate of 1.0 kN/s and sensitivity of 0.5kN. The FS value was obtained based on the average of three test results. After rejecting the tested results with biases exceeding 15%, the UCS was calculated from the average of more than five test results.

### XRD and SEM analysis

Ten- or twenty-grams post-experiment samples were extracted to analyze hydrated products and microstructure using XRD and SEM, respectively. The reaction-terminated samples were ground into powder (< 80 μm) and then dried to a constant weight in a vacuum dryer (30±2°C). All samples were then transferred into vacuum bags, and sealed by a sucking pump to improve the accuracy of microscopic monitoring. After that, the prepared sample was examined by a Rigaku D/Max-2500 XRD, Cu-Kα (1.541874 Å), with a scanning range of 5~80° and a scanning speed of 10°/min. The quantitative phase analysis of paste was performed using the Rietveld refinement method and the analyzed result was obtained by HighScore Plus 4.1 software in Semi-automatic mode, allowing 1% fluctuation in unit cell parameters.

A series of programs on test and analysis microstructure and morphology were carried out through SEM (F20005, JSM-IT500LV, JEOL Ltd) for exploring the microstructure and the morphology of products. The samples were sprayed with gold for the observation under SEM with the magnification from $10^3$ to $10^4$. The operation conditions were of 30 kV with a working distance from 9.1 to 13.7mm.

**TG and DTG analysis**

The effects of SMA content on the hydration products were investigated through TG and DTG analysis. The sample preparation process was similar to that of XRD test. The test temperature ranged from a relatively low temperature (35±0.5°C) to approximately 1000°C, and the temperature rising rate was set as 10°C/min.

**Isothermal calorimetry analysis**

The hydration heat evolutions of the manufactured carbonate-based cementitious material were tested for 84 hours with a constant temperature at 20 °C by an isothermal calorimeter (TAM Air 8-Channel Standard Volume Calorimeter). The test sample was prepared with the same water cement ratio as the strength test in order to minimize the experimental error.

**Pore size distribution analysis**

The 3-day and 28-day samples were selected to analysis the pore size distribution. After drying in vacuum, the samples are degassed at 65 ℃ for 2 hours. The pore size distributions of samples are measured using a $N_2$ absorption device with a pore size range from 0.35 mm to 500 mm and a test precision of ±1% (Type SSA-4000, Beijing, China). The Brunauer-Emmett-Teller (BET) measurement data of samples is analyzed by Barrett-Joyner-Halenda (BJH) model which is suitable to calculate the medium pore diameter (2-100 nm) distribution.

## RESULTS AND DISCUSSIONS

### Mechanical properties

The measured strength values and the calculated strength growth rate of paste with various LP/SMA ratios under different curing ages are exhibited in Fig. 2. It indicates that there is a same trend of variation of UCS and FS. Under IC conditions, the FS/UCS ratio of paste fluctuates uniformly between 0.2~0.3. In Fig. 2, the UCS and FS values of the pastes increased significantly with the decrease in LP/SMA ratio (10/1 ~ 2/1) at the curing ages of 3-day. When the LP/SMA ratio further decreased to 1/1, the UCS and FS of the pastes decreased. Thus, the paste cured for 3-day reached the optimum mechanical properties as the LP/SMA ratio of 2/1, and the maximum UCS and FS were 31.5 MPa and 13.9 MPa, respectively. It also implies that adding a certain amount of SMA could significantly contribute to the development of the mechanical properties of the paste.

With the curing time further lengthened to 14 and 28-day, the UCS and FS values of the pastes with high LP/SMA (10/1 and 7.5/1) decreased with the decrease of the LM/SMA ratio and the increase of the curing time. In contrast, the trends of UCS and FS values of the low LP/SMA (5/1, 3/1, and 2/1) pastes at 14 and 28-day with decreasing LP/SMA ratio are consistent with its variation pattern at 3-day. Meanwhile, the UCS and FS of the pastes with the LP/SMA ratio of 2/1 remained the maximum values at 14 and 28-day. As the curing time increased from 3-day to 14-day, the UCS and FS reached 40.3 MPa and 15.4 MPa, respectively, about 27.9% and 10.8% higher than those of the 3-day pastes. When the curing time was further lengthened to 28-day, the UCS and FS could achieve 49.7MPa and 15.9MPa, respectively, with a growth rate of 57.8% and 14.4% with respect to the 3-day pastes. It is noteworthy that the 3-day strength of paste with the LP/SMA ratio of ~2/1 is 1.4 times that of OPC-52.5 levels for the same period and achieved the equivalent level of strength value at 28 days. Its FS value is much higher than that of Grade 52.5 Portland cement in the same period, which contributed

by a tighter microstructure.[44]

The decrease of LP/SMA ratio means the increase of SMA content. When the LP/SMA ratio (10/1 and 7.5/1) of paste is high, the low dose of SMA reduces the hydration reaction with LP. The micro-aggregate effect formed by a large amount of unreacted LP contributes a certain early strength but is not enough to promote mechanical properties development. As the LP/SMA ratio (5/1, 3/1, and 2/1) decreases, the increased SMA content promotes the hydration reaction between SMA and LP. More hydrolytic SMA increases the alkalinity in system while promoting the dissolution of LP, which promotes the hydration reaction and then improves the mechanical properties. As the LP/SMA ratio (1/1) further decreases, the excessive admixture of SMA leads to rapid condensation in this system, which hinders the hydration process to some extent and weakens the strength development.[45]

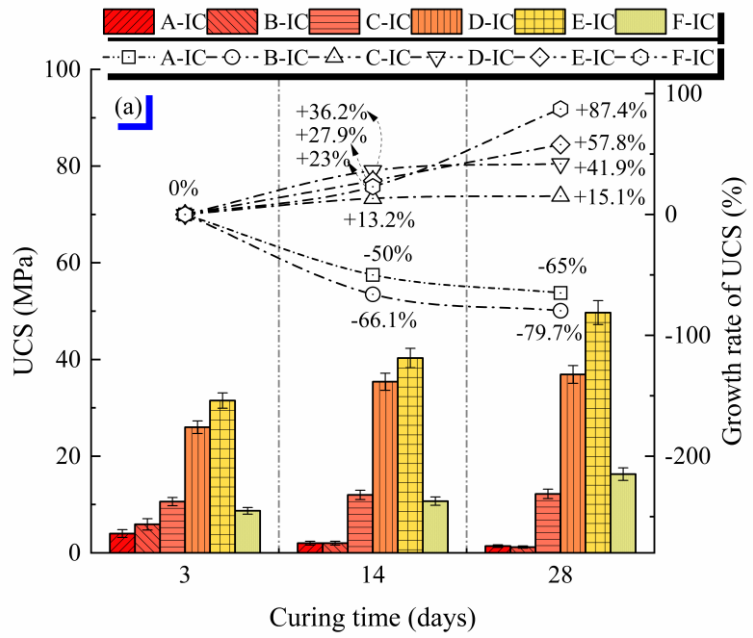

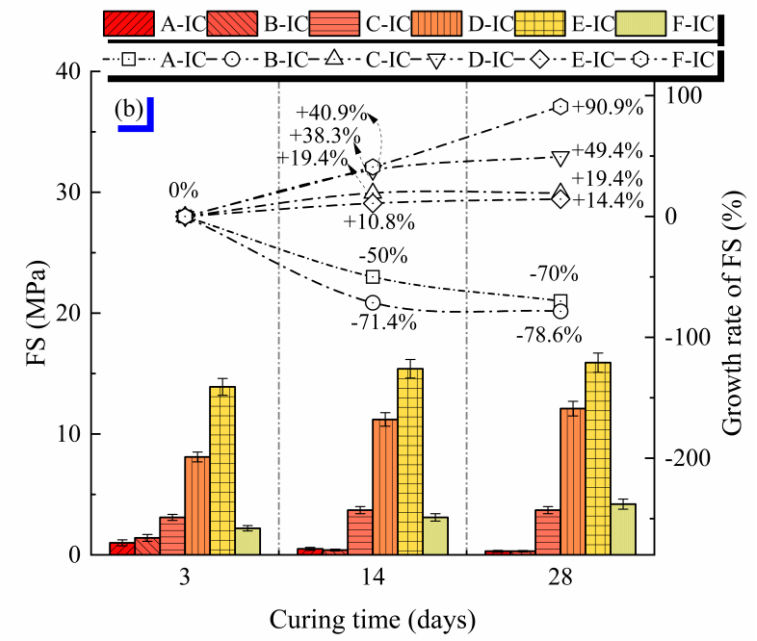


**Fig. 2.** Mechanical properties (a) UCS and (b) FS of the formed pastes with various LP/SMA ratios at different curing times.

The effects of curing conditions on strength development of pastes with three selected LP/SMA ratios (3/1, 2/1, and 1/1) are exhibited in Fig. 3 and 4. It is obvious that, irrespective of curing time and LP/SMA ratio, the specimen at IC demonstrates the highest strength value, which is followed by the specimen at SC. While, the specimen at SC-60 °C has the lowest strength value. Furthermore, for the specimens at IC and SC, the strength value increased with the increase of curing time. However, this trend was obviously not suitable for the specimen at SC-60 °C, which in some cases showed a downtrend in the strength with the increase of curing time. For instance, when LP/SMA ratio was 2/1, the 28-day UCS exhibited increases of 57.8% and 43.8%, respectively, for the specimens at IC and SC, while a decrease of 17.3% for the specimen at SC-60 °C, in comparison with the corresponding 3-day UCS.

Thus, the IC is the best curing environment and plays an important role in strength development. Conversely, SC-60 °C is the weakest curing environment. Specifically, SC-60 °C provides more moisture and higher temperature than that cured in other conditions. The developed high-humidity and high-temperature curing environment induces the partial dissolution and transformation of the

hydration product phase of the carbonate-based cementitious material, thus generating more volume of low-strength sodium carbonate hydrate due to the introduced condition of high-humidity. The presence of sodium carbonate hydrate consumes parts of carbonate while reducing the proportion of other hydration product phase formed. The new combination of hydration product phases builds a weaker microstructure, so it is not conducive to the development of strength.[46]

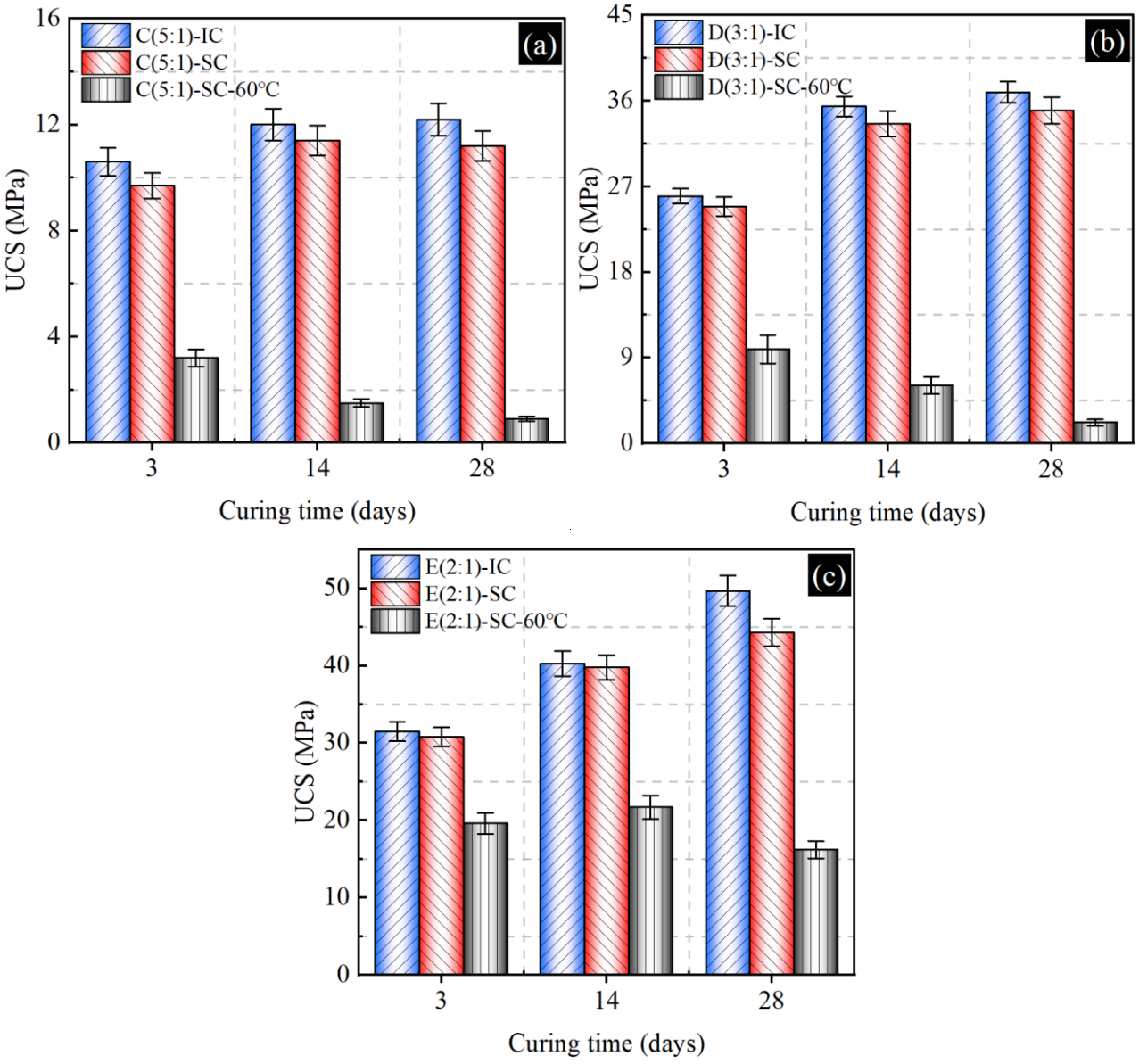


**Fig. 3.** The UCS of paste with various LP/SMA ratios (a) 5/1, (b) 3/1 and (c) 2/1 at different curing times.

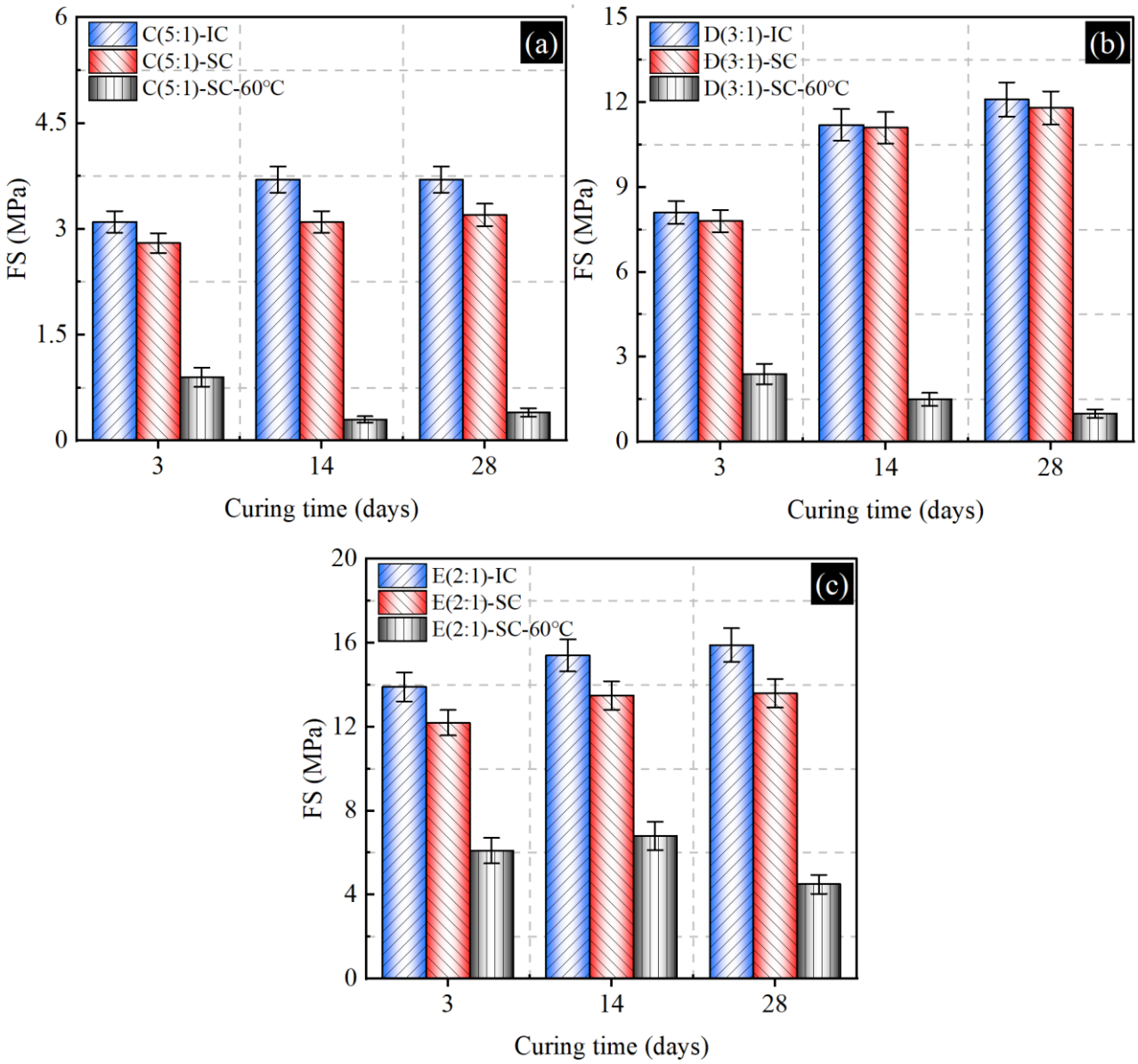


**Fig. 4.** The FS of paste with various LP/SMA ratios (a) 5/1, (b) 3/1 and (c) 2/1 at different curing times.

## Hydrated products and TG-DTG analysis

The XRD patterns of the measured paste with various LP/SMA ratios at 3 and 28 days are exhibited in Fig. 5. Fig. 5a demonstrates that the same phases that produced by the hydration at different LP/SMA were calcium aluminum carbonate hydroxide hydrate (CACHH, $Ca_4Al_2(CO_3)(OH)_{12}\cdot 5H_2O$), unreacted calcium carbonate, sodium calcium carbonate hydrate, sodium carbonate hydrate and aluminum gel.

In addition, other products were also formed from the hydration of paste with different LP/SMA ratios. When the LP/SMA ratio was 10/1 and 7.5/1, sodium calcium carbonate pentahydrate appeared

as a high-water content product phase due to the low dose of SMA. As the LP/SMA reduced to 5/1, a small amount of sodium carbonate monohydrate crystals was generated in the hydration products due to the high concentration of $Na^+$ accumulated by increasing SMA.[36,45] When the LP/SMA ratio declined to ~3/1, the increasing SMA intensified the hydration of calcium carbonate, which induces the contraction of sodium calcium carbonate pentahydrate to sodium calcium carbonate dihydrate. While the ratio of LP/SMA decreased to 2/1 and 1/1, its composition remained consistent. It indicates that the increase of SMA no longer forms new phases and only affects the yield of hydration products.

The peak intensity of calcium carbonate weakened with the decline in the LP/SMA ratio. It indicates the increase of SMA accelerates the consumption of calcium carbonate. Meanwhile, the intensity of CACHH peak (011) of the paste increased with the decrease of LP/SMA (from 10/1 to 2/1), but was not suitable for the ratio of LP/SMA (1/1). This is consistent with the variations in strength as shown in Fig. 2. This, to some extent, indicates that the formation of CACHH contributes to the mechanical properties. However, whether CACHH is the main physical phase supporting the strength development needs to be analyzed in depth, which would be verified in the subsequent sections. Moreover, partial results of the XRD experiments were consistent with that of raw material (Fig. 1), specifically silicon dioxide, calcium magnesium carbonate. In addition, the presence of aluminum hydroxide was mainly due to the hydrolysis of SMA.

Fig. 5b shows that the samples at 28-day were dominated by the typical products observed in the corresponding samples at 3-day. The main difference is that the yield of reacted products increases with the increase of curing time. Also, a decrease in the peak intensity of calcium carbonate was observed in 28-day specimens compared with 3-day samples. This verifies the decomposition of calcium carbonate in-depth.[43,45,47]

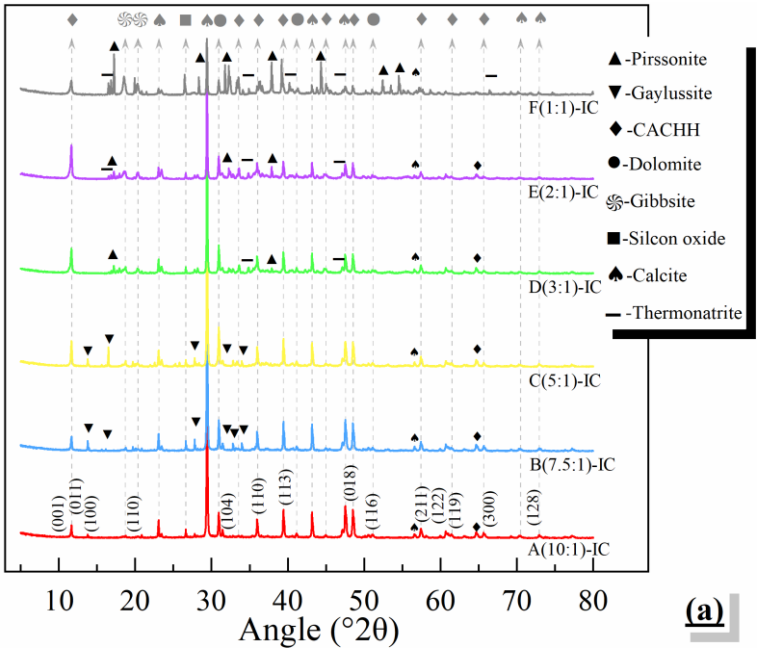


256

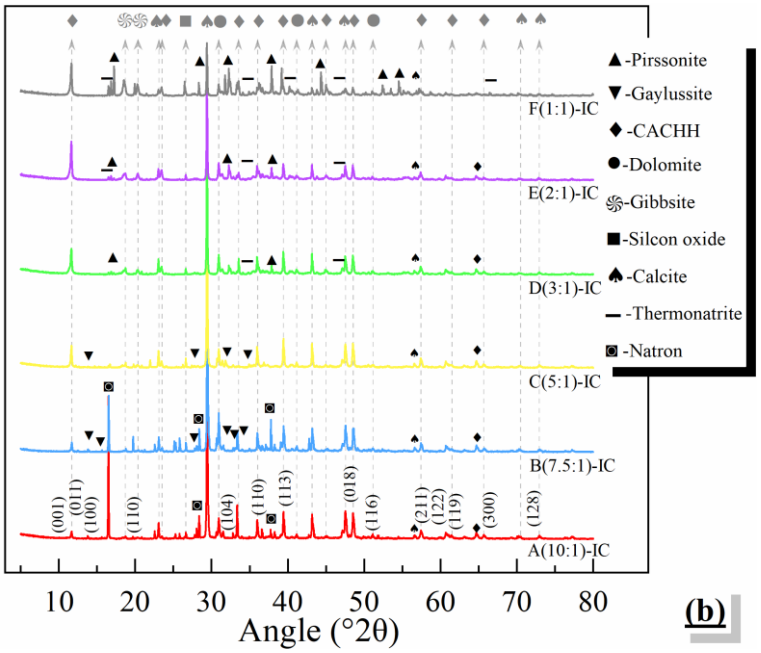


257

258 **Fig. 5.** The XRD patterns of the produced paste from (a) 3d and (b) 28d, with various LP/SMA ratios on IC.

259 The XRD results of the paste with the LP/SMA ratio of 3/1 and 2/1 at various curing conditions are
260 exhibited in Fig. 6. It shows that there was no significant difference between the hydration products
261 formed under IC and SC conditions. Compared with IC and SC conditions, the paste formed in SC-
262 60 °C generated more sodium carbonate monohydrate. This trend was more obvious with the increase
263 of curing time, which may be due to the incorporation of steam promotes crystal formation. Previous
264 study indicated that the alkaline carbonates produce internal stresses to damage the compressive

strength as its volume is larger than that initially occupied by water.[34]

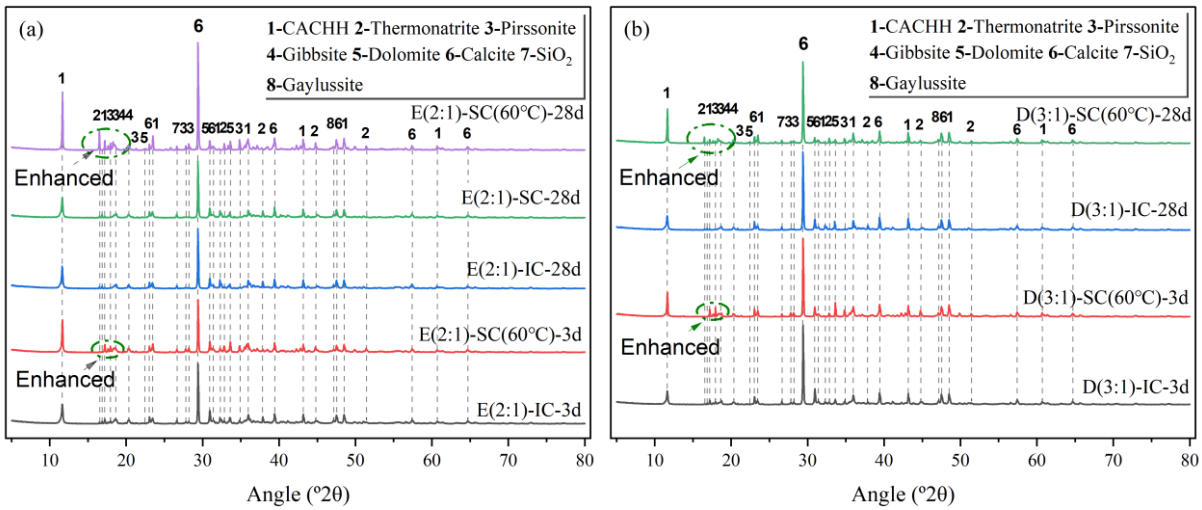


**Fig. 6.** The XRD patterns of the produced paste with various curing condition at 3d and 28d, using the LP/SMA ratio of (a) ~2/1, and (b) ~3/1.

Fig. 7 exhibits the TG-DTG result of 3-day paste with different LP/SMA ratios, and the results of 28-days paste is presented in Fig. 8. Multiple exothermic peaks and significant mass loss occurred in the formed paste with the increase of temperature, in which the quality loss of each sample fluctuated between 46.81~52.14%. When the temperature rose to 280 ℃, the two distinct exothermic peaks was mainly related to the dehydration products (Fig. 7). Aluminum hydroxide dissolved with increasing temperature after the dehydration process finished. The mass loss range of this stage was 18.5~26%. While the temperature rose from 280 ℃ to 690 ℃, the exothermic peak was closely related to the reduction of carbonate and the condensation of hydroxyl, and the range of mass loss in this stage reached 6~13.5%. Then, when the temperature rose from 690 ℃ to 870 ℃, a strong exothermic peak associated with the dehydration of calcium carbonate appears and also, dolomite and sodium carbonate were gradually decomposed.[40,44,46] The loss of mass within this temperature stage ranged from 20.5 to 35.5 %.

The comparison of different samples shows that before 280°C, there is a certain degree of difference in the dehydration stage of all samples, which is related to the degree of hydration of the reaction product (Fig. 7). Between 280°C and 690°C, the mass loss of all samples is basically the same. In the

range of 690°C to 870°C, the mass loss of samples with LP/SMA of 5/1 is the largest, which is related to the more unreacted calcium carbonate content in the paste. The above results can also be clearly seen from the decomposition rate peak of calcium carbonate in fig. 7b. The thermogravimetric results of paste remain unchanged except that the weight loss ratio decreased with the extension of curing time (fig. 8). This means that the main phase of paste has not changed significantly, and the results are consistent with XRD results. The results and the XRD results verify that the content of unreacted calcium carbonate decreases with the increase of SMA, and the formation of more hydration product phase CHAHH has a more favorable contribution to mechanical properties.

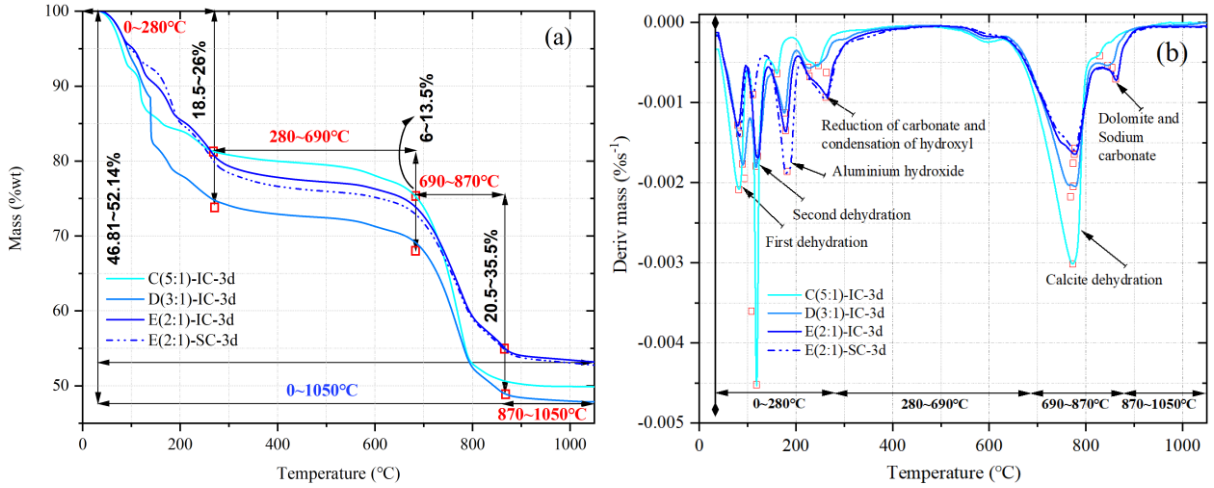


**Fig. 7.** The (a).TG and (b). DTG curve of 3-day paste over temperature changes.

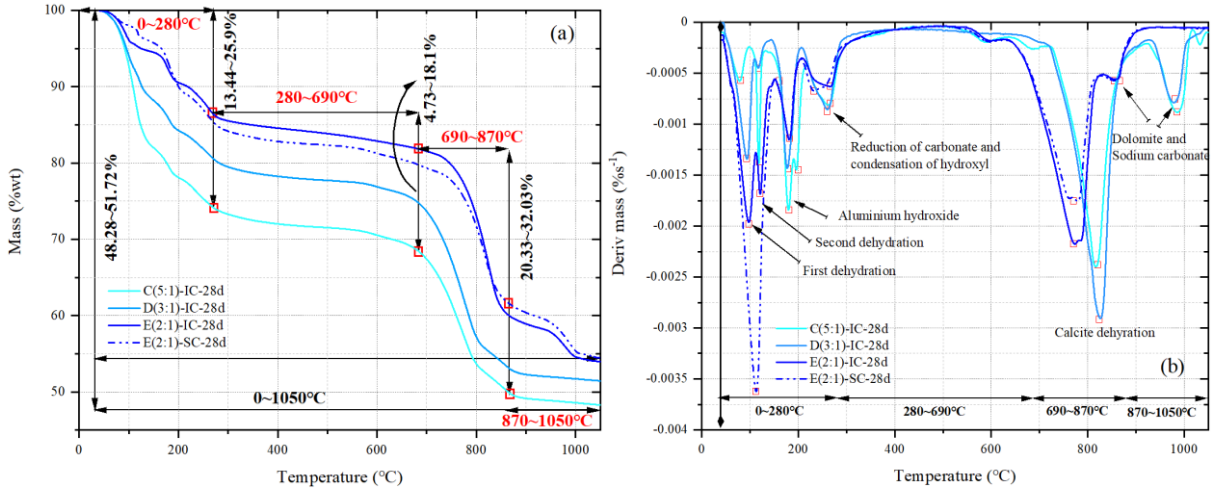


**Fig. 8.** The (a).TG and (b). DTG curve of 28-day paste over temperature changes.

## SEM results and nitrogen adsorption analysis

The SEM images of the measured paste with various LP/SMA ratios at 3-day and 28-day in the IC

condition are exhibited in Fig. 9. In the paste with high LP/SMA ratio (10/1 and 7.5/1), the hydration reaction of low- dose SMA and LP produced a small amount of large-grained CACHH, which formed the loose microstructure with abundant unreacted calcium carbonate. As the LP/SMA ratio in the paste decreased (5/1, 3/1, 2 /1), the large dose of SMA accelerated the hydration reaction with LP to generate a large amount of small-grained CACHH, forming a layered double hydroxides structure. The results for Energy Dispersive Spectrometer verify the formation of CACHH according to Ca-Al ratio, as shown in Fig. 9. With the further reduction of the LP/SMA ratio (1/1) in the paste, the excessive incorporation of SMA caused rapid coagulation and agglomeration of a large amount of calcium carbonate, forming a poor layered microstructure.[17,28,48]

The 28-day microstructure of the paste with LP/SMA ratios of ~10/1 and ~7.5/1 was still looser and more porous compared to 3-day. It also verified the results of the mechanical properties of strength at this ratio. Whereas, as the decrease of LP/SMA ratio (5/1~1/1), the microstructure of paste at 28-day had a denser structure and a more compact crystal morphology than that of 3-day, which was consistent with the development of mechanical properties.

The SEM images of the measured paste with the LP/SMA ratio of 2/1 at 3-day and 28-day in the IC and SC-60 ℃ condition are shown in Fig. 10. In comparison with, in IC condition, the SEM plots of the hydration products under SC-60 °C showed that the microstructure of the paste gradually gelatinized with increasing curing age. This is in agreement with the deterioration of strength and the XRD results (Fig. 10). Thus, the IC is proved to be the best curing environment plays an important role in microstructure of the paste. In contrast, SC-60 ℃ as the most weaken curing environment was verified by Figs. 4, 6 and 10. The high temperature and humidity at SC-60 ℃ induced the gelation of CACHH and promoted the precipitation of sodium carbonate crystals, which in turn destroyed the layered microstructure and led to the generation of a gel state with a lower strength, exhibiting a

deterioration of mechanical properties.[49-50]

Combining the analysis of XRD and strength results, the content of CACHH increased with the decrease of LP/SMA (excluding the 1/1 case), and the decrease of micropore and grain size promoted the layered structure of CACHH to constitute a tighter microstructure in a progressive manner. The micro-bridge effect produced by the formation of sheet-like LDHs significantly improved the mechanical properties, especially in the FS values.[20,28]

The adsorption-desorption curve and pore size distribution of the E-IC sample cured in 3-day and 28-day are shown in Fig. 11. The whole volume of the selected sample deceases insignificantly with the increase of curing age. Based on Fig. 11a, the 3-day adsorption-desorption volume is about 25.6 cc/g, which is 2.21 times higher than that of 28-day volume. It means that the pore volume significantly shrink due to the more hydration products has been formed and then filled fully the pore. To further investigate the changes in the pore size distribution of the selected sample at the different curing ages. According to Fig. 11b, all the pore are significantly reduced with the curing age lasting from 3-day to 28-day. More specifically, the microscopic pore can be filled fully with the hydration product and then its volume hardly disappears. Therefore, fewer pores imply a denser microstructure, which also indicates a significant increase in hydration products. And the increase of the lamellar product phase and the decrease of the pores provide the microscopic basis for the enhancement of the mechanical properties. The mentioned results are consistent with the development of mechanical properties and product phases, which provide a powerful foundation for the hydration of carbonate-based cementitious materials.

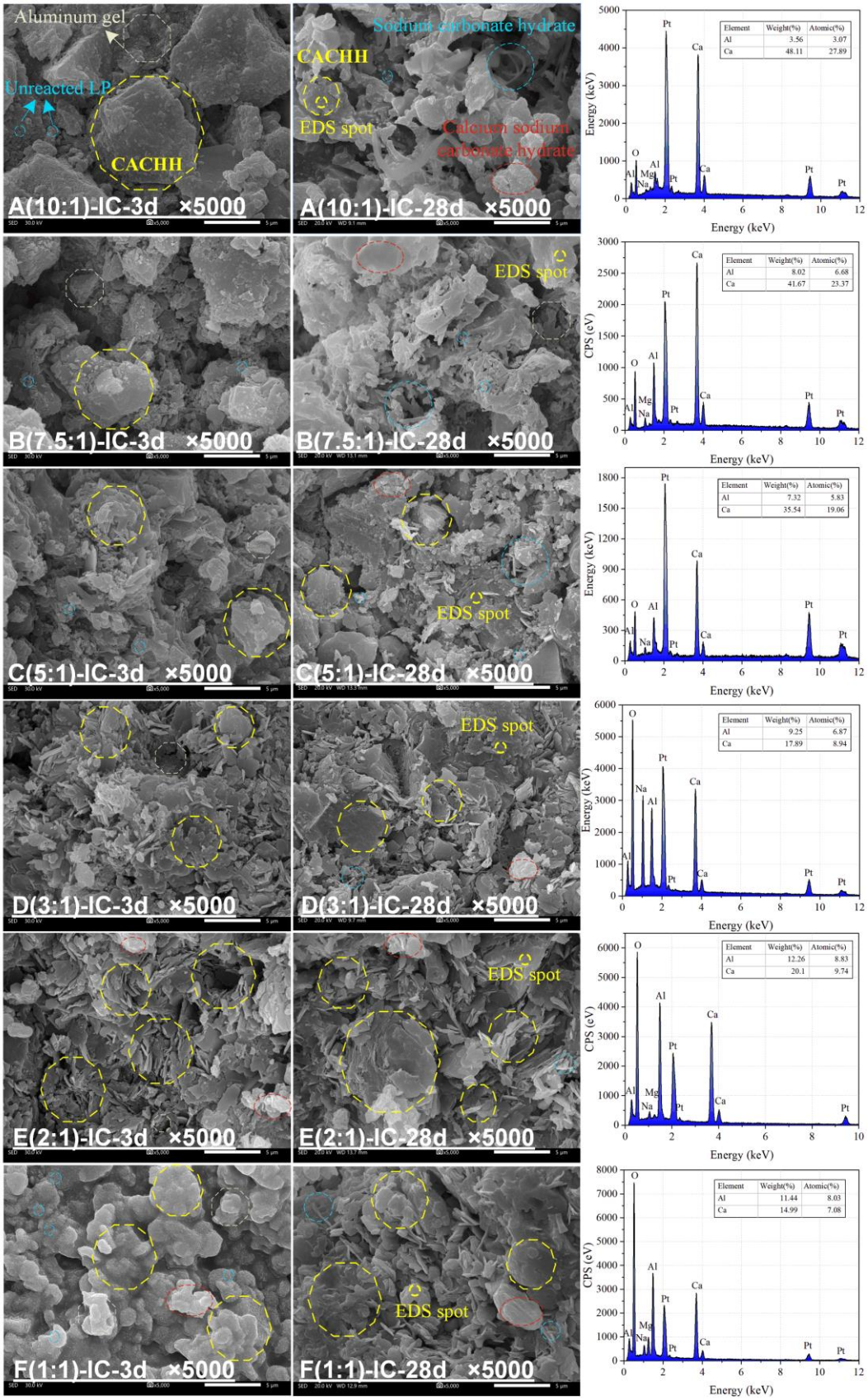


**Fig. 9.** The SEM pattens of the formed paste with various LP/SMA ratios on IC at 3d and 28d.

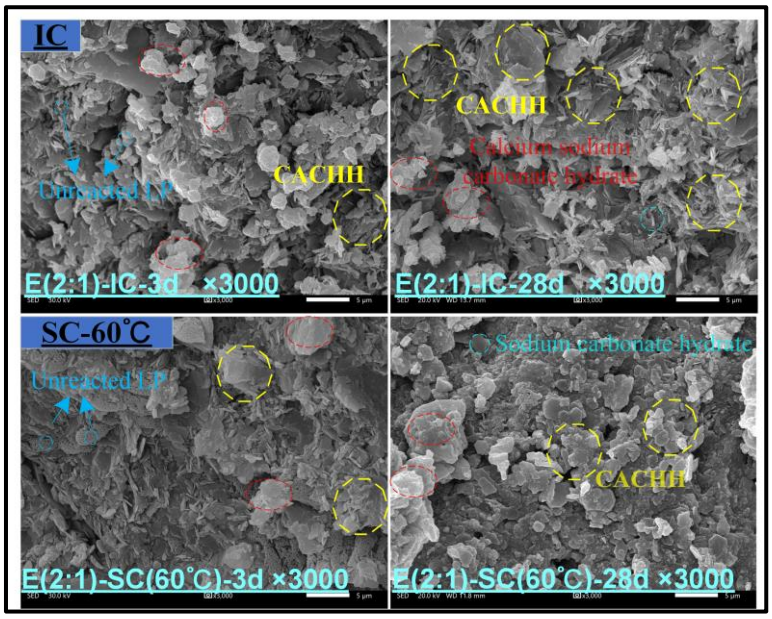


343

344 **Fig. 10.** The SEM pattens of the paste with the LP/SMA ratio of 2/1 on IC and SC-60 ℃ at 3-d and 28-d.

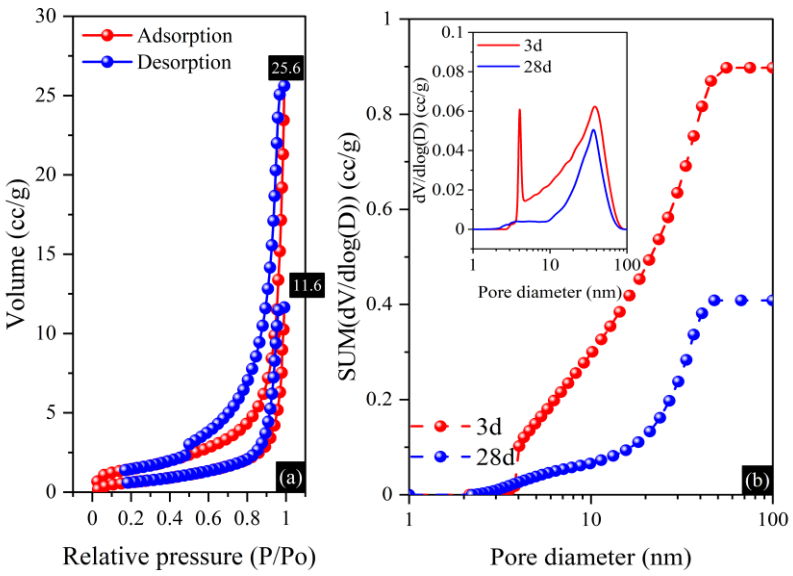


345

346 **Fig. 11.** The nitrogen adsorption test results (a) Adsorption-desorption curve and (b) Pore size distribution

347 of the E-IC sample cured in 3-d and 28-d.

348

349 **Connections between the main hydration products and UCS and FS**

350 The relationship between UCS values and the production of CACHH is shown in Fig. 12. The

351 CACHH content was calculated by the converting results of XRD. Fig. 12a and b indicates the

352 measured UCS values have a linear relationship with the CACHH content under the action of IC.

This implies that the increase of CACHH has a positive contribution to accelerating the structure formation of LDHs. As the CACHH content continued to increase, the LDHs structure continued to layer and stack to form a tighter microstructure, and this dense structure provided a powerful explanation for the excellent mechanical properties.

In addition, the effect of CACHH content on UCS values of the paste with the LP/SMA ratio of ~2/1 at different curing conditions is exhibited in Fig. 12c. It denotes that there is a significant linear relationship between the strength of the paste and the product CACHH under IC and SC, which illustrates the direct contribution of CACHH to the mechanical properties. The high humidity provided by SC-60 °C produces a carbonate-like substance that is detrimental to strength development, resulting in a reduced linear relationship between the CACHH formed and strength.

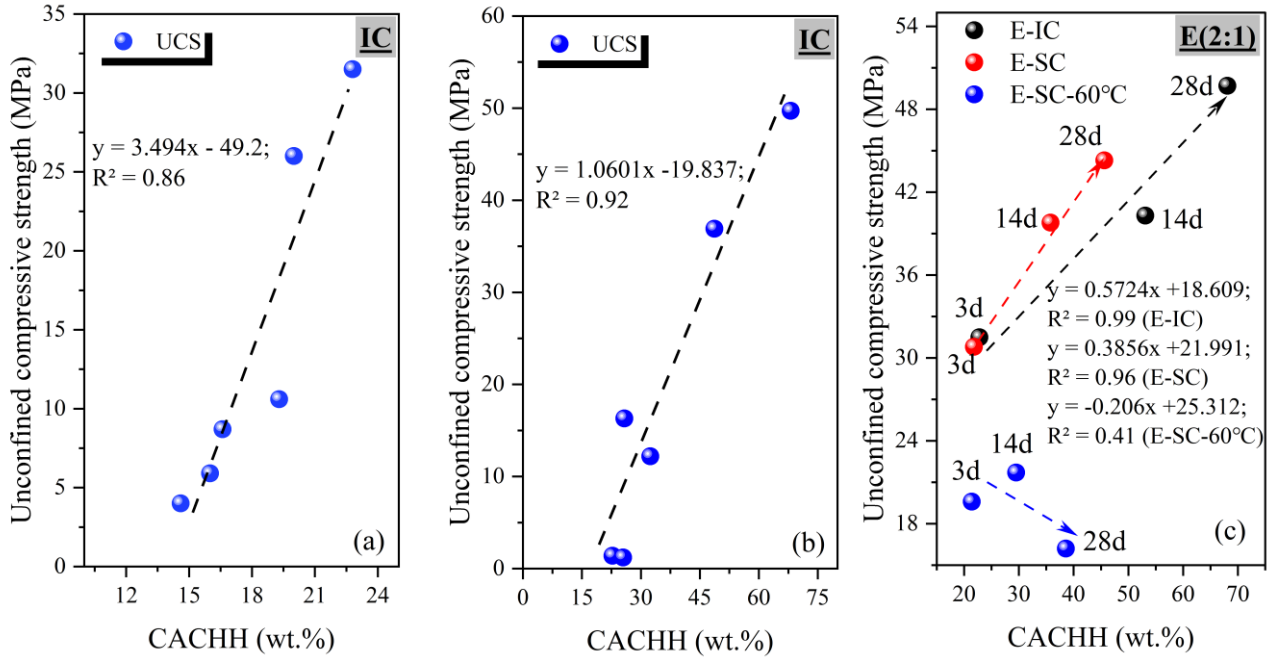


**Fig. 12.** Relationship between UCS and CACHH content at (a)3d, (b)28d, and (c) LP/SMA ratio of 2/1.

**Environmental impact and energy consumption**

The carbon dioxide equivalent index was employed to estimate the environmental impact of raw material and formed carbonate-based cementitious material. The eco-mechanical index is calculated

according to Eq. (1-4), which can accurately reflect the environmental impact caused by the formed paste.

$$CI\text{-}UCS = \frac{PUM_{CO_2\text{-}e}}{f_{UCS}} \quad (1)$$

$$CI\text{-}FS = \frac{PUM_{CO_2\text{-}e}}{f_{FS}} \quad (2)$$

$CI\text{-}UCS$ and $CI\text{-}FS$ stand for the carbon emissions (kg/MPa • $m^3$) contributed by unit UCS, and FS, respectively. $PUM_{CO_2\text{-}e}$ represents the carbon emissions of per unit mass (kg/$m^3$). $f_{UCS}$ and $f_{FS}$ denote the UCS and FS, respectively.

$$EI\text{-}UCS = \frac{PUM_{KJ\text{-}C}}{f_{UCS}} \quad (3)$$

$$EI\text{-}FS = \frac{PUM_{KJ\text{-}C}}{f_{FS}} \quad (4)$$

$EI\text{-}UCS$ and $EI\text{-}FS$ exhibits the energy consumption (MJ/MPa • $m^3$) contributed by unit UCS and FS, respectively. $PUM_{KJ\text{-}C}$ expresses the energy consumption of per unit mass (MJ/$m^3$). A unit mass was used for the environmental impact analysis since the densities of the samples are almost identical. The carbon emissions of per unit mass employed in this study were obtained from previous literature.[50-52] Specifically, the carbon emissions and energy consumption per unit mass of ordinary Portland cement clinker were 0.83 $CO_2$ • kg/kg and 4.727 MJ/kg, respectively.[53-54] The carbon emissions and energy consumption per unit mass of limestone powder were 0.017 $CO_2$ • kg/kg and 0.35 MJ/kg, respectively. [53-54] While the carbon emissions and energy consumption per unit mass of SMA were 1.26 $CO_2$ • kg/kg and 5.81 MJ/kg, respectively, which was provided by the manufacturers.

The carbon emissions and energy consumption of raw materials incurred by formed paste with different LP/SMA ratios are shown in Fig. 13. In terms of carbon emissions, the carbon emissions per unit mass of Portland cement produced are higher than that required to manufacture the same mass

of paste (Fig. 13a). Thus, the paste with low carbon emissions can minimize the contribution of cementitious materials to the greenhouse effect during the production process. Fig. 13b indicates the energy consumption required to produce carbonate-based cementitious material is much lower than that of Portland cement. Furthermore, the carbon emissions and energy consumptions of the formed paste increase with the decrease of LP/SMA ratio due to increasing the dosage of SMA. In conclusion, the fabrication for carbonate-based cementitious material without calcination and mechanical activation, resulting in a low carbon and energy consumption for its preparation. This also indicates that the formed carbonate-based cementitious material is a very environmentally friendly and energy-saving cementitious material.

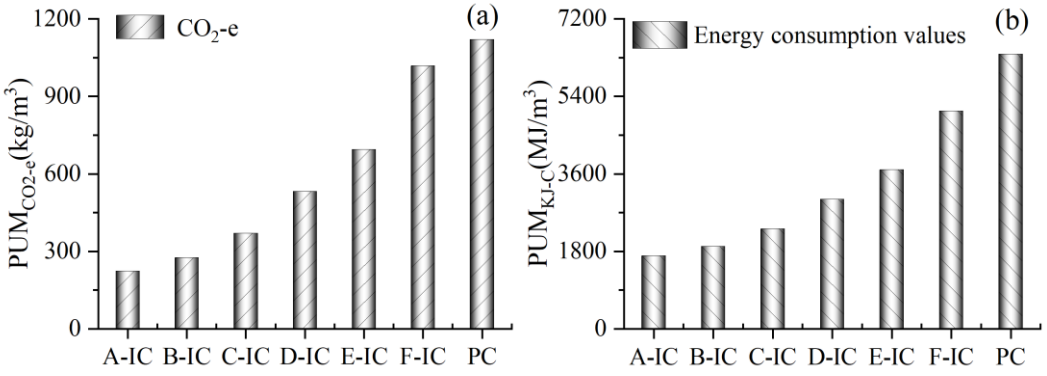


**Fig. 13.** (a) Carbon emissions and (b) energy consumption of paste with different LP/SMA ratios.

The CI-UCS and CI-FS results of paste with various LP/SMA ratios at 28 days are shown in Fig. 14. It is evident that the trends of both CI-UCS and CI-UCS maintain a fundamental consistency, which is intimately dependent on the mechanical properties. When the LP/SMA ratio (10/1 and 7.5/1) in the paste was high, the lower UCS led to bigger CI-UCS values. As the LP/SMA ratio (5/1, 3/1, and 2/1) in the paste decreased, the increased SMA content improved the mechanical properties and decreased the CI-UCS and CI-FS values. With the LP/SMA ratio (1/1) reaching extremely low, the deterioration of mechanical properties again increased the CI-UCS and CI-FS values. In terms of the analysis of the paste with the LP/SMA of 2/1, the lowest CI-UCS and CI-FS of the formed paste were

13.97 and 43.67, respectively, meaning that the incorporation of the appropriate amount of SMA can promote the balance between the environmental impact and mechanical properties. Compared with Portland cement, although the increase in SMA leads to an increase in carbon emissions and energy consumption, it equally improves the mechanical properties and significantly reduces the CI-UCS and CI-FS values. Therefore, the paste prepared at the ratio of LP/SMA (5/1, 3/1 and 2/1) has extremely low CI-UCS and CI-FS, which implied that the prepared carbonate-based cementitious material had high value utilization and low environmental impact.

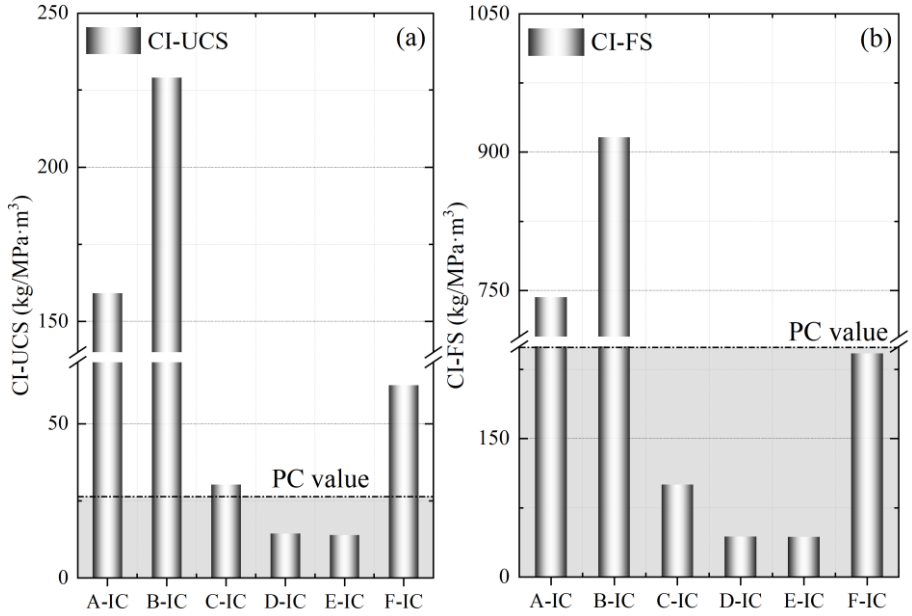


**Fig. 14.** (a) CI-UCS and (b) CI-FS of the formed paste with different LP/SMA ratios at 28 days in the IC.

The EI-UCS and EI-FS values of paste with various LP/SMA ratios at 28 days during the IC condition are shown in Fig. 15. As can be seen from Fig. 15, influence of the LP/SMA ratio on EI-UCS and EI-FS values is highly consistent with that of LP/SMA ratio on CI-UCS and CI-FS values due to the similarity of calculation principles. Also, the lowest EI-UCS values (74.29) and lowest EI-FS values (232.22) were observed when the LP/SMA value was 2/1. Compared with Portland cement, the paste prepared with the ratio of LP/SMA (5/1, 3/1, and 2/1) has extremely low EI-UCS and EI-FS. It implies that the formed paste has less energy consumption per unit volume and achieves high-value utilization of resources.

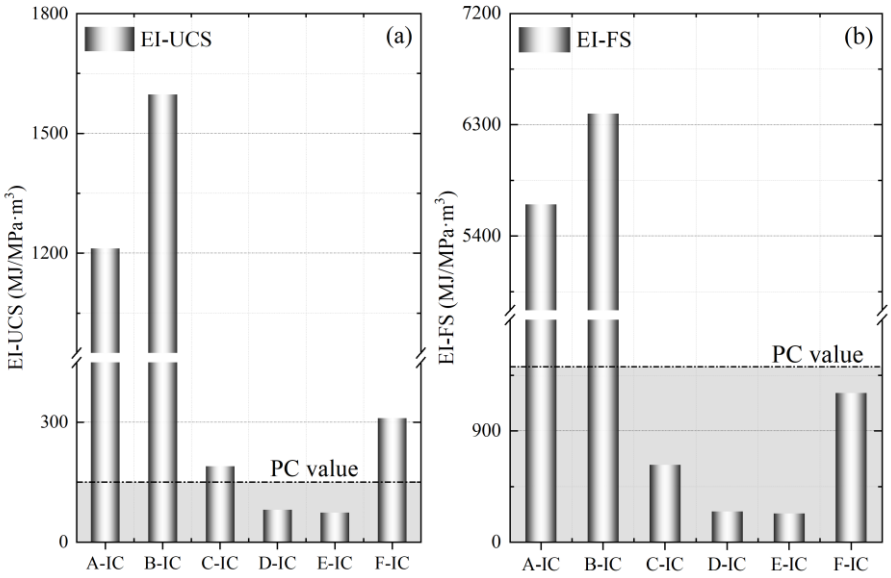


**Fig. 15.** (a) EI-UCS and (b) EI-FS of the formed paste with different LP/SMA ratios at 28 days in the IC.

## Early hydration analysis

The peak strength of the paste formed appeared under the LP/SMA ratio of 2/1. The IC condition provided a suitable temperature and low humidity environment for the formation of hydration products of paste, and thus contribute an excellent development environment for the evolution of strength.[18,46] The hydration heat and the pore size distribution of the E-IC sample are exhibited in Figs. 15, 16 and 17, respectively. In combination with the results of hydration exothermic and pore size distribution, the hydration products and microstructure development processes were analyzed in-depth. The hydration reaction under IC condition can be mainly divided into the following three stages (Figs. 16 and 17).

Stage I, namely the dissolving stage, where SMA was firstly dissolved in water with hydrolysis reaction (Eq. (5)) and a small amount of calcium carbonate dissolution reaction (Eq. (6)). [16,46] This could also be confirmed in the hydration exothermic results, in which the peak 1 occurred in the early exothermic stage about 3~5 minutes. The maximum rate of heat release during this stage reached about 80.3 mW/g, which indicates that the strong chemical dissolution reaction takes place at this stage. Therefore, at this stage, when the water is added to this system, the main heat release is root in

the rapid dissolution of SMA and the very small amounts dissolution of calcium carbonate.

$$AlO_2^- + 2H_2O \rightarrow Al(OH)_4^- \quad (5)$$

$$CaCO_3 \xrightarrow{\text{micro-reaction}} Ca^{2+} + CO_3^{2-} \quad (6)$$

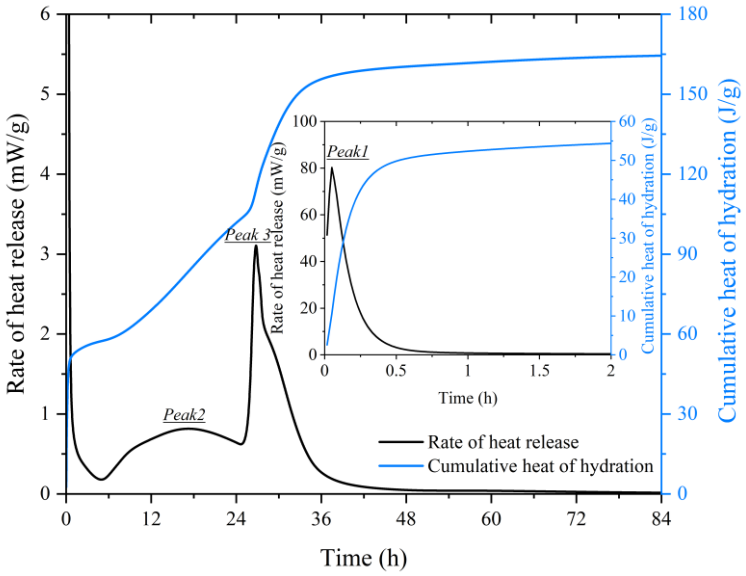


**Fig .16.** The hydration exothermic curve of E-IC was measured by isothermal calorimetry (20°C).

Stage II, called the formation stage of layered double hydroxides (LDHs) structure, in which the formed $Al(OH)_4^-$ reacted with calcium carbonate and free $Ca^{2+}$ to generate the LDHs structure and released a large amount of heat to further accelerate the dissolution reaction in the stage I. Refer to the Eq. (7) for the specific reaction process. The same process was validated in the exothermic process of hydration, and as can be observed in Fig. 16, the exothermic peak 2 was observed as the hydration advanced. It was observed to be a continuous exothermic process different from the rapid dissolution in the early stage. The continuous exothermic heat at this stage corresponds to the initial formation and development of the structure of LDHs.

$$2Ca^{2+} + Al(OH)_4^- + 2OH^- \rightarrow \left[Ca_2Al(OH)_6\right]^+ \quad (7)$$

Stage III, entitled the formation stage of the final hydration product. In this stage, the LDHs further reacted carbonate and water molecules for forming the layered CACHH gel based on the Eq. (8).[40,44]

In addition, under the action of the high temperature generated in the second stage, $Na^+$ in the system reacted with calcium carbonate and water molecules to produce sodium calcium carbonate hydrate, as detailed in Eq. (9). The final formation of hydration products was also observed in the hydration exothermic curve. The appearance of the hydration exothermic peak 3 signalized the final formation of layered CACHH and the formation of sodium calcium carbonate hydrate in this stage.

$$2\left[Ca_2Al(OH)_6\right]^+ + CO_3^{2-} + 5H_2O \rightarrow Ca_4Al_2(OH)_{12}CO_3 \cdot 5H_2O \quad (8)$$

$$2Na^+ + Ca^{2+} + 2CO_3^{2-} + nH_2O \rightarrow Na_2Ca(CO_3)_2 \cdot nH_2O \quad (9)$$

The formed CACHH, originally known as the tetra-calcium dialuminium hydroxide carbonate pentahydrate, is also known in environmental chemistry field as hydrocalumite or Friedel's salt, is commonly called in cement-based disciplines as single-carbon AFm.[49] The CACHH is a layered compound constructed by positively charged main layers and negatively charged interlayers, in which the $Al^{3+}$ and $Ca^{2+}$ are six and seven oxygen coordinated, respectively.[20,50] The development of mechanical properties of the pastes can be explained from the microstructure and chemical composition of CACHH. Firstly, CACHH products with layered structure can contribute on a certain strength. With the superposition and compounding of the layered structure, the strength of performed paste is rapidly increased. In addition, undissolved calcium carbonate is encapsulated in the layered double hydroxides structure as micro-particles, which provides nucleation sites and promotes the improvement of mechanical properties. Finally, the densification of the layered structure reduces the porosity, which improves the strength significantly.[9,15]

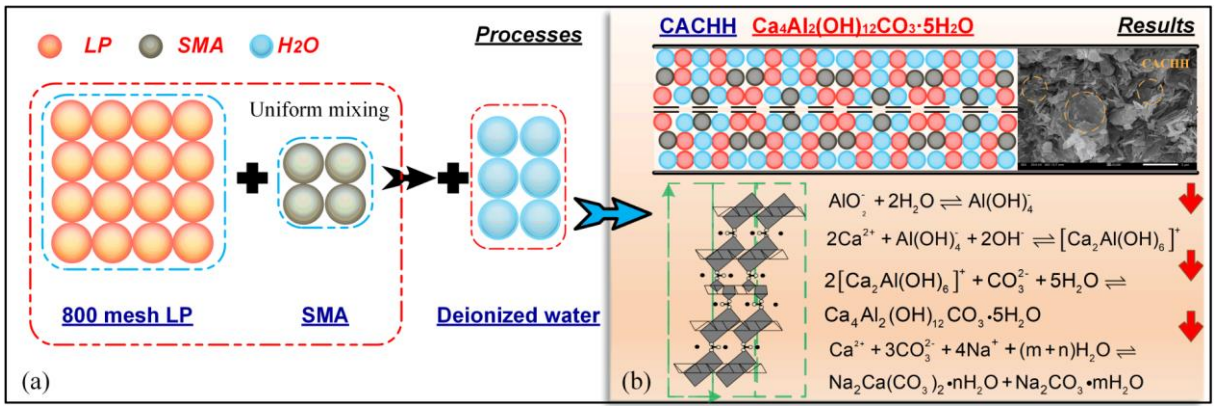


**Fig. 17.** A simple chemical strategy to fabricate paste based on various LP/SMA mass ratios and different curing conditions (a) the fabricating process and (b) the fabricating result.

Interestingly, the strength of cementitious products formed by different LP/SMA ratios existed a significantly difference. On the one hand, it can be attributed to the amount of CACHH products and the densification of the layered structure. On the other hand, the best mechanical properties are related to the ratio of Ca/Al in CACHH. The closer the Ca/Al ratio is to 2/1, the better the mechanical properties of the paste. However, when the ratio of Ca/Al is much greater than 2/1, the reaction between calcium carbonate and SMA is weakened. Excessive water molecules participate in the Eq. (9) to obtain more hydrate with high binding water.

Sodium calcium carbonate pentahydrate is produced during the hydration as the LP/SMA is 7.5/1 and 5/1 (Fig. 2). When the LP/SMA ratio is less than 5/1, the reaction between LP and SMA is enhanced, and less water molecules participate in the Eq. (9) to obtain the hydrates, that is, sodium calcium carbonate dihydrate is generated during the hydration. However, when the LP/SMA ratio is 10/1, it can completely react with a small part LP at the initial stage and due to the extremely small SMA, which may not be enough to further generate sodium calcium carbonate. With the increase of curing time, the continuous hydration reduces LP and promotes CACHH increase. In addition, the existence of sodium salt and humidity promotes the precipitation of sodium carbonate crystals (Fig. 15b), which is fully reflected in results of 28 d (Fig. 2).

It is worth noting that variations in curing conditions mainly affect the temperature and humidity.

The curing environment of SC is basically the same as that of IC, and the small difference in humidity promotes the generation of carbonate products, as detailed in Eq. (6). The SC condition is not conducive to the layered development of CACHH; thus, its mechanical properties are slightly reduced (Fig. 17). Compared with IC, SC-60 ℃ has a significant difference in temperature and vapor content. On the one hand, the formation of sodium calcium carbonate hydrate and the precipitation of sodium carbonate crystal has been obviously promoted, leading to the increase of crystallinity and crystalline grain size and, thus causing interference to the layered distribution of CACHH. On the other hand, the decrease of CACHH yield is also an important reason for the weakening of mechanical properties. The decausticization was intensified due to the increase in the formation of sodium carbonate, which was not conducive to the development of mechanical properties.[8,12,17,44] Meanwhile, the increased content of $Na^+$ in this system, which promoted the reaction (Eq. (10)) and was also not conducive to the development of macroscopic mechanical properties.

$$Ca^{2+} + 3CO_3^{2-} + 4Na^+ + (m+n)H_2O \rightarrow Na_2Ca(CO_3)_2 \cdot nH_2O + Na_2CO_3 \cdot mH_2O \quad (10)$$

## CONCLUSIONS

In conclusion, we proposed a simple chemical preparation method of carbonate-based cementitious material, formed by calcium carbonate and SMA under room environment (20±2 °C) without pre-calcination treatment, showing a potential approach to address limestone waste. The produced paste is a very environmentally friendly and energy-saving cementitious material. Results provide a new perspective for the application of LP in civil engineering and render reference for the solid waste value-added utilization of LP. Specific conclusions are as below:

1) When the LP/SMA ratio was 2/1, the maximum UCS and FS of the 28-day pastes under IC were 49.7 MPa and 15.9 MPa, respectively. The IC is the best curing condition, the 28-day UCS increases

of 57.8% and 43.8%, respectively, for the specimens at IC and SC, while a decrease of 17.3% for the specimen at SC-60 ℃, in comparison with the corresponding 3-day UCS.

2) The CACHH is the main hydration products of the paste at different LP/SMA. The content of CACHH increased with the decrease of LP/SMA (from 10/1 to 2/1), indicates that the formation of CACHH contributes to the mechanical properties. Compared with IC and SC conditions, the paste formed in SC-60 ℃ generated more sodium carbonate monohydrate which in turn destroyed the layered microstructure and led to the generation of a gel state with a lower strength. Thus, the sample cured in SC-60 ℃ is not conducive to the development of mechanical properties.

3) The increase in SMA consumes LP to form a dense LDHs consisting of CACHH. The micro-bridge effect developed by LDHs significantly increases the flexural strength of specimens. The undissolved calcium carbonate is encapsulated in the LDHs structure as micro-particles, which provides nucleation sites and promotes the improvement of mechanical properties. The optimum LP/SMA and curing condition accelerates the densification of microstructure, which reduces porosity and significantly enhances UCS and FS values.

4) The carbon emissions and energy consumptions of the produced paste increase with the decrease of LP/SMA ratio due to increasing the dosage of SMA. The carbon emissions per unit mass of ordinary Portland cement produced are higher than that of the same mass of paste. The fabricated paste with LP/SMA of 2/1 has an extremely low CI-UCS and EI-UCS (13.97 and 43.67), suggesting that the prepared paste is a very environmentally friendly and energy-saving cementitious material.

Although the synthesis conditions of paste are described in this paper along with the basic mechanical property formation and development patterns and environmental impact evaluation. The influence of water-cement ratio and pH value on the paste needs to be further studied. In addition, the temperature stability and workability of this paste have not been explained and analyzed, pointing to

546 further research.

## 547 CONFLICTS OF INTEREST

548 The authors declare no competing financial interests.

## 549 ACKNOWLEDGEMENTS

550 The authors appreciate the financial support from Hunan Province Key Field R&D Program (Grant
551 No.2020wk2005), and the Postgraduate Scholarship, Central South University, Changsha, China.

## 552 CREDIT AUTHOR STATEMENT

553 **Fan Wang:** Conceptualization**,** Data curation, Writing-Original draft, and Writing-review & editing;
554 **Guangcheng Long**: Funding acquisition, Project administration, and Validation; **Jionghuang He:**
555 Writing-Reviewing and Editing; **Youjun Xie:** Supervision and Formal analysis; **Zhuo Tan:** Writing-
556 review & editing; **Xiang Zhou:** Formal analysis; **Min Bai:** Investigation and Validation; **JohnL Zhou:**
557 Formal analysis, Methodology and Conceptualization, Writing-review & editing.

## 558 REFERENCES

559 (1) Huang, Y.; Ji, Y.; Kang, Z.; et al. Integrating eggshell-derived $CaCO_3$/MgO nanocomposites and chitosan into
560 a biomimetic scaffold for bone regeneration. Chem. Eng. J. **2020**, 395, 125098.
561 https://doi.org/10.1016/j.cej.2020.125098.
562 (2) Kamkum, P.; Vittayakorn, W.; Seeharaj, P.; et al. Utilization of eggshell as a low-cost precursor for synthesizing
563 calcium niobate ceramic. Green. Mater. **2018**, 6(3), 108-116. https://doi.org/10.1680/jgrma.18.00049.
564 (3) Hassan, T.; Rangari, V. K; Jeelani, S. Value-added biopolymer nanocomposites from waste eggshell-based
565 CaCO3 nanoparticles as fillers. ACS Sustainable Chem Eng. **2014**, 2(4), 706-717.
566 https://doi.org/10.1021/sc400405v.
567 (4) Zhao, Y. Z.; Habraken, W.; Galina, M.; et al. A hydrated crystalline calcium carbonate phase: Calcium carbonate
568 hemihydrate. Science. **2019**, 363(6425), 396-400. https://doi.org/10.1126/science.aav0210.
569 (5) Beck, J. W.; Edwards, R. L.; Ito, E.; et al. Sea-surface temperature from coral skeletal strontium/calcium ratios.
570 Science. **1992**, 257(5070), 644-647. https://doi.org/10.1126/science.257.5070.644.
571 (6) Gebauer, D.; Volkel, A.; Colfen, H. Stable prenucleation calcium carbonate clusters. Science. **2008**, 322(5909),

572 1819-1822. https://doi.org/10.1126/science.1164271.
573 (7) Nielsen, M. H.; Aloni, S.; Yoreo, J. D. In-situ TEM imaging of $CaCO_3$ nucleation reveals coexistence of direct
574 and indirect pathways. Science. **2014**, 345 (6201), 1158-62. https://doi.org/10.1126/science.1254051.
575 (8) Wang, D.; Wang, Q.; Huang, Z. Reuse of copper slag as a supplementary cementitious material: reactivity and
576 safety. Resour. Conserv. Recy. **2020**, 162, 105037. https://doi.org/ 10.1016/j.resconrec.2020.105037.
577 (9) Mu, Y.; Liu, Z.; Wang, F. Comparative study on the carbonation-activated calcium silicates as sustainable
578 binders: Reactivity, mechanical performance, and microstructure. ACS. Sustainable. Chem. Eng. **2019**, 7(7),
579 7058-7070. https://doi.org/10.1021/acssuschemeng.8b06841.
580 (10)Li, C.; Wu, M.; Yao, W. Eco-efficient cementitious system consisting of belite-ye'elimite-ferrite cement,
581 limestone filler, and silica fume. ACS Sustainable Chem. Eng. **2019**, 7(8), 7941-7950.
582 https://doi.org/10.1021/acssuschemeng.9b00702.
583 (11)Choi, S. G.; Chu, J.; Brown, R. C.; Wang, K.; Wen, Z. Sustainable bio-cement production via microbially
584 induced calcium carbonate precipitation: use of limestone and acetic acid derived from pyrolysis of
585 lignocellulosic biomass. ACS Sustainable Chem. Eng. **2017**, 5(6), 5183-5190.
586 https://doi.org/10.1021/acssuschemeng.7b00521.
587 (12)Wang, Y.; Xu, M.; Yang, L.; et al. Pressure-stabilized divalent ozonide $CaO_3$ and its impact on Earth's oxygen
588 cycles. Nat. Commun. **2020**, 11(1), 4702. https://doi.org/10.1038/s41467-020-18541-2.
589 (13)Juenger, M.; Siddique, R. Recent advances in understanding the role of supplementary cementitious materials
590 in concrete. Cem. Concr. Res. **2016**, 78, 71-80. https://doi.org/10.1016/j.cemconres.2015.03.018.
591 (14)Arora, A.; Sant, G.; Neithalath, N. Ternary blends containing slag and inter-ground/blended limestone:
592 Hydration, strength, and pore structure. Constr. Build. Mater. **2016**, 102, 113-124.
593 https://doi.org/10.1016/j.conbuildmat.2015.10.179.
594 (15)Pan, J. L.; Cai, J. M.; Ma, H.; et al. Development of multiscale fiber-reinforced engineered cementitious
595 composites with PVA fiber and $CaCO_3$ whisker. J. Mater. Civil. Eng. **2018**, 30(6), 04018106.
596 https://doi.org/10.1061/(asce)mt.1943-5533.0002305.
597 (16)Matschei, T.; Lothenbach, B.; Glasser, F. P. The role of calcium carbonate in cement hydration. Cement.
598 Concrete. Res. **2007**, 37(4), 551-558. https://doi.org/10.1016/j.cemconres.2006.10.013.
599 (17)Wang, Y.; He, X.; Su, Y.; et al. Effect of aluminium phases on thaumasite formation in cement slurries containing
600 limestone powder, Mag. Concrete. Res. **2018**, 70(12), 610-616. https://doi.org/10.1680/jmacr.16.00521.
601 (18)Camiletti, J.; Soliman, A. M.; Nehdi, M. L.; et al. Effects of nano- and micro-limestone addition on early-age
602 properties of ultra-high-performance concrete. Mater. Struct. **2013**, 46(6), 881-898.

https://doi.org/10.1617/s11527-012-9940-0.

(19)Irassar, E. F. Sulfate attack on cementitious materials containing limestone filler — A review. Cem. Concr. Res. **2009**, 39(3), 241-254. https://doi.org/10.1016/j.cemconres.2008.11.007.

(20)Bentz, D. P.; Ardani, A.; Barrett, T.; et al. Multi-scale investigation of the performance of limestone in concrete. Constr. Build. Mater. **2015**, 75, 1-10. https://doi.org/10.1016/j.conbuildmat.2014.10.042.

(21)He, J.; Long, G.; Ma, C.; Ma, K.; Xie, Y.; Shi, Y. Effect of triethanolamine on hydration kinetics of cement–fly ash system at elevated curing temperature. ACS Sustainable Chem. Eng. **2020**, 8(27), 10053-10064. https://doi.org/10.1021/acssuschemeng.0c01763.

(22)Cao, M.; Ming, X.; He, K.; et al. Effect of Macro-, Micro- and Nano-Calcium carbonate on properties of cementitious composites-A review. Materials (Basel). **2019**, 12(5), 781. https://doi.org/10.3390/ma12050781.

(23)Bentz, D.P.; Ferraris, C.F.; Jones, S.Z.; et al. Limestone and silica powder replacements for cement: early-age performance. Cem. Concr. Comp. **2017**, 78, 43-56. https://doi.org/10.1016/j.cemconcomp.2017.01.001.

(24)Goergens, J.; Manninger, T.; Goetz-Neunhoeffer, F. In-situ XRD study of the temperature-dependent early hydration of calcium aluminate cement in a mix with calcite. Cem. Concr.. Res. **2020**, 136, 106160. https://doi.org/10.1016/j.cemconres.2020.106160.

(25)He, J.; Long, G.; Ma, K.; Xie, Y.; Cheng, Z. Improvement of the hydration of a fly Ash–cement system by the synergic action of triethanolamine and C–S–H seeding. ACS Sustainable Chem. Eng. **2021**, 9(7), 2804-2815. https://doi.org/10.1021/acssuschemeng.0c08618.

(26)Rakhimova, N.R.; Rakhimov, R.Z.; Naumkina, N.I.; et al. Influence of limestone content, fineness, and composition on the properties and microstructure of alkali-activated slag cement, Cem. Concr. Comp. **2016**, 72, 268-274. https://doi.org/10.1016/j.cemconcomp.2016.06.015.

(27)Galan, I.; Andrade, C.; Castellote, M. Natural and accelerated $CO_2$ binding kinetics in cement paste at different relative humidities. Cement. Concrete. Res. **2013**, 49, 21-28. https://doi.org/10.1016/j.cemconres.2013.03.009.

(28)Wang, D.; Shi, C.; Farzadnia, N.; et al. A review on use of limestone powder in cement-based materials: Mechanism, hydration and microstructures. Constr. Build. Mater. **2018**, 181, 659-672. https://doi.org/10.1016/j.conbuildmat.2018.06.075.

(29)Castellote, M.; Llorente, I.; Andrade, C. Influence of the composition of the binder and the carbonation on the zeta potential values of hardened cementitious materials. Cem. Concr. Res. **2006**, 36(10), 1915-1921. https://doi.org/10.1016/j.cemconres.2006.05.033.

(30)Péra, J.; Husson, S.; Guilhot B. J. C. Composites, Influence of finely ground limestone on cement hydration. Cem. Concr. Comp. **1999**, 21(2), 99-105. https://doi.org/10.1016/S0958-9465(98)000201.

(31)Chang, Z. Y.; Long, G. C.; Zhou, J. L.; et al. Valorization of sewage sludge in the fabrication of construction and building materials: A review. Resour. Conserv. Recy. **2020**, 154, 104606. https://doi.org/10.1016/j.resconrec.2019.104606.

(32)Moesgaard, M.; Herfort, D.; Steenberg, M.; et al. Physical performances of blended cements containing calcium aluminosilicate glass powder and limestone. Cem. Concr. Res. **2011**, 41(3), 359-364. https://doi.org/10.1016/j.cemconres.2010.12.005.

(33)Chen, J.; Liang, C.; Li, B.; et al. The effect of nano-$\gamma Al_2O_3$ additive on early hydration of calcium aluminate cement. Constr. Build. Mater. **2018**, 158, 755-760. https://doi.org/10.1016/j.conbuildmat.2017.10.071.

(34)Ortega-Zavala, A.; Santana-Carrillo, A.; Burciaga-Díaz, B.; et al. An initial study on alkali activated limestone binders. Cem. Concr. Res. **2019**, 120, 267-278. https://doi.org/10.1016/j.cemconres.2019.04.002.

(35)Coppola, B.; Palmero, P.; Montanaro, L.; et al. 2020. Alkali-activation of marble sludge: Influence of curing conditions and waste glass addition. J. Eur. Ceram. Soc. **2020**, 40(11), 3776-3787. https://doi.org/10.1016/j.jeurceramsoc.2019.11.068.

(36)Palomo, A.; Krivenko, P.; Garcia-Lodeiro, I.; et al. A review on alkaline activation: new analytical perspectives. Mater. Construc. **2014**, 64(315), 140-159. https://doi.org/10.3989/mc.2014.00314.

(37)Provis, J. L. Alkali-activated materials, Cem. Concr. Res. **2018**, 114, 40-48. https://doi.org/10.1016/j.cemconres.2017.02.009.

(38)Choudhary, J.; Kumar, B.; Gupta, A. Application of waste materials as fillers in bituminous mixes. Waste Manage, **2018**, 78, 417-425. https://doi.org/10.1016/j.wasman.2018.06.009.

(39)Francois, M.; Renaudin, G.; Evrard, O. A cementitious compound with composition $3CaO.\ Al_2O_3.\ CaCO_3.\ 11H_2O$. Acta Crystallographica Section C: Crystal Structure Communications. **1998**, 54(9), 1214–1217. https://doi.org/10.1107/S0108270198004223.

(40)Renaudin, G.; Rapin, J.P.; Humbert, B.; et al. Thermal behaviour of the nitrated AFm phase $Ca_4Al_2(OH)_{12}(NO_3)_2•4H_2O$ and structure determination of the intermediate hydrate $Ca_4Al_2(OH)_{12}(NO_3)_2•2H_2O$. Cem. Concr. Res. **2000**, 30(2), 307-314. https://doi.org/10.1016/s0008-8846(99)00251-3.

(41)Kou, X.; Guo, H.; Ayele, E. G.; Li, S.; Zhao, Y.; Wang, S.; Ma, X. Adsorption of $CO_2$ on MgAl-$CO_3$ LDHs-derived sorbents with 3D nanoflower-like structure. Energy. Fuels, 2018, 32(4), 5313-5320. https://doi.org/10.1021/acs.energyfuels.8b00024.

(42)Cwirzen, A. An alkali activated limestone concrete composition and use of composition in concrete casting. Europen Patent Ofce EP 2 514 727 A2. **2012**. https://www.freepatentsonline.com/ EP2514727B1.html

(43)Ipavec, A.; Gabrovšek, R.; Vuk, T.; et al. Carbo-aluminate phases formation during the hydration of Calcite-

containing Portland cement. J. Amer. Ceram. Soc. **2011**, 94(4), 1238-1242. https://doi.org/10.1111/j.1551-2916.2010.04201.x.

(44)Lothenbach, B.; Kulik, D.A.; Matschei, T.; et al. Cemdata18: A chemical thermodynamic database for hydrated Portland cements and alkali-activated materials. Cem. Concr. Res. **2019**, 115, 472-506. https://doi.org/10.1016/j.cemconres.2018.04.018.

(45)Jiao, H. Z.; Wang, S. F.; Wu, A. X.; et al. Cementitious property of $NaAlO_2$-activated Ge slag as cement supplement. Int. J. Min. Met. Mater. **2019**, 26(12), 1594-1603. https://doi.org/10.1007/s12613-019-1901-y.

(46)Borges, O.H.; Santos, T.; Salvini, V.R.; et al. $Al_2O_3$–CaO macroporous ceramics containing hydrocalumite-like phases. Ceram. Int. **2020**, 46(5), 5929-5936. https://doi.org/10.1016/j.ceramint.2019.11.046.

(47)Briendl, L.G.; Mittermayr, F.; Baldermann, A.; et al. Early hydration of cementitious systems accelerated by aluminium sulphate: Effect of fine limestone. Cem. Concr. Res. **2020**, 134, 106069. https://doi.org/10.1016/j.cemconres.2020.106069.

(48)Renaudin, G.; Francois, M.; Evrard, O. Order and disorder in the lamellar hydrated tetracalcium monocarboaluminate compound. Cem. Concr. Res. **1999**, 29(1), 63-69. https://doi.org/10.1016/S0008-8846(98)00184-7.

(49)Wu, Y.; Chi, Y.; Bai, H.; et al. Effective removal of selenate from aqueous solutions by the Friedel phase. J. Hazard. Mater. **2010**, 176(1-3), 193-208. https://doi.org/10.1016/j.jhazmat.2009.11.012.

(50)Goh, K. H.; Lim, T. T.; Dong, Z. Application of layered double hydroxides for removal of oxyanions: a review. Water. Res. **2008**, 42(6-7), 1343-68. https://doi.org/10.1016/j.watres.2007.10.043.

(51)Yang, K, H.; Song, J, K.; Song, K, I. Assessment of $CO_2$ reduction of alkali-activated concrete. J. Clean. Prod. **2013**, 39, 265–272. https://doi:10.1016/j.jclepro.2012.08.001.

(52)Bontempi, E. A new approach for evaluating the sustainability of raw materials substitution based on embodied energy and the $CO_2$ footprint. J. Clean. Prod. **2017**, 162, 162-169. https://doi:10.1016/j.jclepro.2017.06.028.

(53)Long, G.; Gao, Y.; Xie, Y. Designing more sustainable and greener self-compacting concrete. Constr. Build. Mater. **2015**, 84, 301–306. https://doi:10.1016/j.conbuildmat.2015.02.072.

(54)Shi, Y.; Long, G.; Ma, C.; Xie, Y.; He, J. Design and preparation of ultra-high performance concrete with low environmental impact. J. Clean. Prod. **2019**, 214, 633–643. https://doi:10.1016/j.jclepro.2018.12.318.

692 **For Table of Contents Use Only:**

693 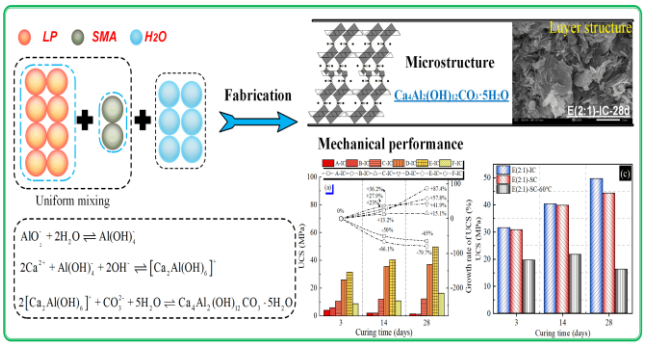


694 High value-added utilization of limestone powder to fabricate calcium carbonate-based cementitious material has

695 lower carbon emission and energy consumption with respect to Portland cement.